AIAA/AAS Astrodynamics Specialist Conference and Exhibit
5-8 August 2002, Monterey, California

AIAA 2002-4909

HIGH-FIDELITY MODELING OF SEMI-AUTONOMOUS ATTITUDE CONTROL DURING AEROBRAKING

Wyatt R. Johnson* and James M. Longuski†
School of Aeronautics and Astronautics, Purdue University
West Lafayette, Indiana 47907-1282
and
Daniel T. Lyons‡
Jet Propulsion Laboratory, California Institute of Technology
Pasadena, California 91109-8099

We investigate the automation of a Mars aerobraking vehicle that uses reaction wheels for attitude and angular momentum control during atmospheric flythrough. In a previous study, single-axis control laws were developed for minimum onboard instrumentation to compensate for large variations in entry time and atmospheric density. In this paper we test modifications of those control laws to provide two-axis control in high-fidelity simulations that include six degrees of freedom, nearly ideal reaction wheels, spherical harmonics, and oblate atmosphere. Preliminary results indicate that our approach may be highly practical for an autonomous aerobraking mission at Mars.

Nomenclature

A	=	Reaction wheel orientation matrix
C	=	Fully normalized tesseral coefficient
D	=	Direction cosine matrix
$\mathbf{H}$	=	Total angular momentum, kg·m^2/s
I	=	Spacecraft inertia matrix, kg·m^2
J	=	Diagonal matrix of reaction wheel moments of inertia, kg·m^2
K_D	=	Reaction wheel drag torque coefficient
L	=	International Astronomical Union (IAU) Latitude, deg
$\mathbf{M}$	=	External moment acting on spacecraft, kg·m^2/s^2
n	=	Number of reaction wheels
P	=	Fully normalized associated Legendre function
$\mathbf{q}$	=	Inertial attitude quaternion
$\mathbf{r}$	=	Inertial position vector of spacecraft, km
S	=	Fully normalized sectoral coefficient
U	=	Gravity potential, km^2/s^2
$\mathbf{u}$	=	Reaction wheel control torques, kg·m^2/s^2
$\mathbf{V}$	=	Inertial velocity vector of spacecraft, km/s
$\mathbf{x}$	=	State vector
α	=	Angle of attack, deg
β	=	Sideslip angle, deg
γ	=	Flight path angle, deg
θ	=	True anomaly plus argument of periapsis, deg
λ	=	IAU Longitude, deg
μ	=	Gravitational parameter, km^3/s^2
ρ	=	Atmospheric density, kg/km^3
χ	=	θ - γ, deg
ψ	=	Roll angle, deg
$\boldsymbol{\Omega}$	=	Reaction wheel angular rates, deg/s
$\boldsymbol{\omega}$	=	Spacecraft angular rates, deg/s

Subscripts

A	=	Affinor of rotation
atm	=	Atmospheric
Q	=	Quaternion kinematical matrix
rel	=	Relative

Superscripts

e	=	Equilibrium
i	=	Inertial
cm	=	Center of mass

*Doctoral Candidate, Student Member AIAA.
†Professor, Associate Fellow AIAA, Member AAS.
‡Senior Engineer, Jet Propulsion Laboratory.

Introduction

AEROBRAKING saved the Mars Global Surveyor (Fig. 1) 1200 m/s of propulsive ΔV in

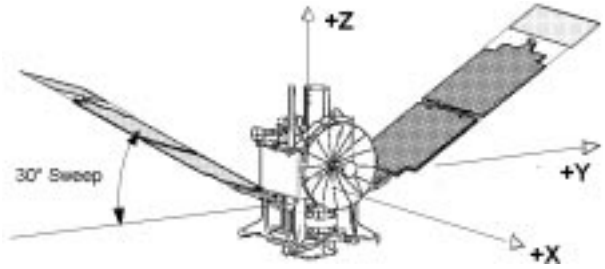

Fig. 1 The Mars Global Surveyor Spacecraft

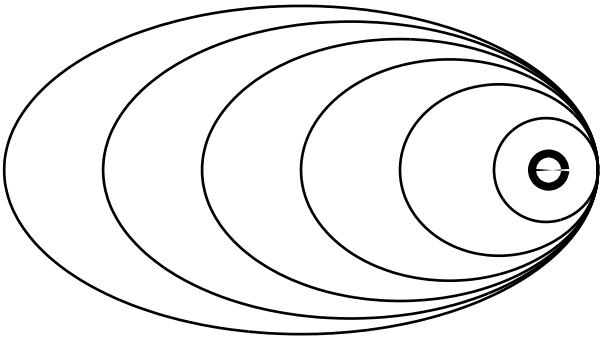

Fig. 2 Orbit decay using aerobraking.

placing a spacecraft into a low-energy orbit around Mars.[1–5] Similar aeroassisted techniques in the literature also provide reduction in propulsive maneuvers.[6–8] The tradeoffs in using aerobraking include increased time before the science phase can begin, increased communications requirements[9] to monitor aerobraking progress, and the necessary dumping of angular momentum accumulated during each drag pass.[10]

Description of Problem

An aerobraking spacecraft uses the atmosphere to reduce the energy of the orbit (Fig. 2). The atmospheric drag force provides the desirable ΔV to effect the orbit change. During each orbit, the spacecraft also accumulates angular momentum from several external torques (e.g. aerodynamic, gravity gradient, solar radiation pressure). Traditionally, the spacecraft reaction wheels absorb this angular momentum, allowing the spacecraft itself to remain in an inertial attitude. As the reaction wheels become saturated, propellant is used to eliminate the acquired angular momentum.[9]

In our scenario, we use the atmospheric moment to our advantage. Instead of acquiring additional momentum during the drag pass, the spacecraft obtains a free desaturation of the reaction wheels by torquing against the atmosphere. Our goal is to devise a control law for the reaction wheels such that the net spacecraft momentum after each flythrough is driven to zero. Ideally, the spacecraft would have sufficient instrumentation available to measure every state variable. Unfortunately, such instrumentation comes at the expense of additional hardware cost and mass to the mission. We therefore choose to find a controller which will only rely on angular rate feedback.

Table 1 Reference spacecraft parameters

Parameter	Reference value
mass	1000 kg
C_D	1.9
C_{M_x}	-0.01 deg^{-1}
C_{M_y}	-0.00366 deg^{-1}
A_{ref}	17.44 m^2
L_{ref}	8.73 m
max rw torque	0.18 N·m
rw capacity	27.0 N·m·s
I_{xx}	814 kg·m^2
I_{yy}	410 kg·m^2
I_{zz}	695 kg·m^2
J	0.0645 kg·m^2

Modeling assumptions

- The only measurable states are spacecraft and reaction wheel angular rates, and the inertial quaternion vector.
- The Martian gravity field is evaluated up to 10th order and degree from a spherical harmonic model.
- The spacecraft has $n \geq 3$ reaction wheels, which span $\mathcal{R}^3$.
- The reaction wheels are aligned in arbitrary (possibly non-orthogonal) orientation, subject to the $\mathcal{R}^3$ constraint.
- The reaction wheels are nearly ideal.[11]
- The atmosphere rotates as a rigid body along with Mars.
- The atmosphere is modeled as oblate and locally exponential (using MarsGRAM COSPAR data[12,13]).
- The controller provides control about the two aerodynamically stable axes only (pitch and yaw). (I.e., no attempt is made to control rotation about the roll axis.)
- The reference spacecraft properties are given in Table 1.

Equations of Motion

Orbital

The inertial position of the spacecraft is described in Cartesian coordinates by the International Astronomical Union (IAU) convention.[14] The inertial $X-Y$ plane is fixed in the equatorial plane of Mars, with the X direction defined by the intersection of the ecliptic and the equator. The Z direction is along the Martian north pole.

The three position Equations of Motion (EOMs) are simply:

$$\dot{\mathbf{r}} = \mathbf{V} \tag{1}$$

The 3 velocity EOM's may be written as:

$$\dot{\mathbf{V}} = \boldsymbol{\nabla} U + \frac{\rho A_{ref} C_D}{2m} \|\mathbf{V}_{rel}\| \mathbf{V}_{rel} \tag{2}$$

where the relative wind on the spacecraft is:

$$\mathbf{V}_{rel} = \mathbf{V}_{atm} - \mathbf{V} \tag{3}$$

and where the atmospheric velocity $\mathbf{V}_{atm}$ is given by:

$$\mathbf{V}_{atm} = -\omega_{atm} y \hat{\mathbf{x}} + \omega_{atm} x \hat{\mathbf{y}} \tag{4}$$

The gravity potential U is given by:

$$U = \frac{\mu}{r}\left\{1 + \sum_{n=1}^{\infty}\sum_{m=0}^{n}\left(\frac{R}{r}\right)^n P_{nm}(\sin L) \times \left[C_{nm}\cos m\lambda + S_{nm}\sin m\lambda\right]\right\} \tag{5}$$

We evaluate the gravity potential up to 10th order and degree, which is needed to resolve the orbital perturbations caused by Olympus Mons.

Attitude

We can express the spacecraft's attitude either inertially (using quaternions), or in terms of relative wind angles (such as angle of attack and sideslip angle). The spacecraft itself will not be able to measure these relative wind angles; but they are important from an analytical point of view, since the momentum EOMs are coupled with the relative wind angle EOMs.

Both sets of attitude EOMs require angular rate information, which is obtained from the momentum EOM. The total system angular momentum consists of two components — one due to the angular rate of the spacecraft relative to the inertial frame, and the other due to the reaction wheels rotating relative to the spacecraft frame. The total momentum is thus:

$${}^{i}\mathbf{H}^{cm} = I\boldsymbol{\omega} + AJ\boldsymbol{\Omega} \tag{6}$$

Since the reaction wheels can only spin about one principal axis, only a single moment of inertia is needed to describe a reaction wheel. The J matrix is an $n \times n$ diagonal matrix of reaction wheel moments of inertia. The A matrix (which is size $3 \times n$) maps unit vectors from the individual reaction wheels to the body-fixed frame.

To develop the attitude EOMs, the momentum vector in Eq. 6 is differentiated with respect to the inertial frame to yield:

$${}^{i}\dot{\mathbf{H}}^{cm} = I\dot{\boldsymbol{\omega}} + AJ\dot{\boldsymbol{\Omega}} + \omega_A\left(I\boldsymbol{\omega} + AJ\boldsymbol{\Omega}\right) \tag{7}$$

The matrix ω_A is the "affinor of rotation", which is the skew-symmetric matrix equivalent to the cross product operation:

$$\omega_A \equiv \begin{bmatrix} 0 & -\omega_z & \omega_y \\ \omega_z & 0 & -\omega_x \\ -\omega_y & \omega_x & 0 \end{bmatrix} \tag{8}$$

With reaction wheel drag torques present, we have:

$$J\dot{\boldsymbol{\Omega}} = \mathbf{u} - K_D\boldsymbol{\Omega} \tag{9}$$

Now we apply Euler's Law, combining Eqs. 7 and 9 to yield:

$$\mathbf{M}^{cm} = I\dot{\boldsymbol{\omega}} + A(\mathbf{u} - K_D\boldsymbol{\Omega}) + \omega_A I\boldsymbol{\omega} + \omega_A AJ\boldsymbol{\Omega} \tag{10}$$

$$\dot{\boldsymbol{\omega}} = I^{-1}\left(\mathbf{M}^{cm} - \omega_A I\boldsymbol{\omega} - \omega_A AJ\boldsymbol{\Omega} - A(\mathbf{u} - K_D\boldsymbol{\Omega})\right) \tag{11}$$

$$\dot{\boldsymbol{\omega}} = I^{-1}\left(\mathbf{M}^{cm} - \omega_A I\boldsymbol{\omega} - \omega_A AJ\boldsymbol{\Omega} - A\mathbf{u} + AK_D\boldsymbol{\Omega}\right) \tag{12}$$

$$\dot{\boldsymbol{\Omega}} = J^{-1}\mathbf{u} - J^{-1}K_D\boldsymbol{\Omega} \tag{13}$$

In this study, the external moment $\mathbf{M}^{cm}$ is simply the atmospheric torque. For the MGS model,[5] the +X axis has a moment proportional to β, and the +Y axis has a moment proportional to α. Thus, the atmospheric torque term is:

$$\mathbf{M}^{cm} = \frac{1}{2}\rho V_{rel}^2 A_{ref} L_{ref} \begin{bmatrix} C_{M_X}(\beta) \\ C_{M_Y}(\alpha) \\ 0 \end{bmatrix} \tag{14}$$

The final form of the momentum EOMs is given by Eqs. 12,13, and 14.

Inertial EOMs

The spacecraft's inertial attitude is determined from:

$$\dot{\mathbf{q}} = \frac{1}{2}\omega_Q \mathbf{q} \tag{15}$$

where

$$\omega_Q = \begin{bmatrix} 0 & \omega_z & -\omega_y & \omega_x \\ -\omega_z & 0 & \omega_x & \omega_y \\ \omega_y & -\omega_x & 0 & \omega_z \\ -\omega_x & -\omega_y & -\omega_z & 0 \end{bmatrix} \tag{16}$$

Relative EOMs

Since the momentum EOMs are a function of the aerodynamic angles α and β (from Eqs. 12 and 14), we need to derive equations of motion for these angles to conveniently analyze the behavior of the system. These EOMs we will derive are not actually integrated in the simulation, since the inertial attitude and position are sufficient to calculate the α and β. The motivation for this analysis is to linearize the relative attitude EOMs for use in a linear feedback controller.

We note that the relative wind angles α and β can be thought of as two Euler angles. These angles are measured relative to the relative wind vector. With $\alpha = \beta = 0$, the spacecraft is pointing directly into the wind. The third Euler angle needed to complete the sequence is roll (ψ, about the +Z spacecraft axis), which must be the first rotation in the sequence. By choosing the second and third rotations as angle of attack (α) and sideslip (β), respectively, the aerodynamic properties of α and β are preserved. This 321 Euler sequence is oriented with respect to the relative wind, which is not inertially fixed. Thus we must include another rotation to transform inertial unit vectors into relative wind vectors. This is accomplished by two coaxial rotations — the first rotating the spacecraft along its orbit through an angle of θ from some inertially fixed point (e.g., the ascending node), and the second rotating the spacecraft's attitude to point along its velocity vector (a rotation through the flight path angle γ). We define the net rotation by the value $\chi \equiv \theta - \gamma$.

The inertial frame directions are chosen to match the spacecraft attitude when $\alpha = \beta = \psi = 0$. This means that $\hat{x}_1$ points to the ascending node of the orbit, $\hat{y}_1$ points away from the orbital momentum vector, and $\hat{z}_1$ completes a right-handed sequence by pointing to a location in the orbital plane 90 degrees ahead of the ascending node. With this definition $\dot{\boldsymbol{\chi}} = -\dot{\chi}\hat{y}_1$.

The direction cosine matrix mapping from inertial coordinates to body-fixed coordinates is:

$$D = D_\beta \cdot D_\alpha \cdot D_\psi \cdot D_\chi \tag{17}$$

where

$$D_\chi = \begin{bmatrix} \cos\chi & 0 & \sin\chi \\ 0 & 1 & 0 \\ -\sin\chi & 0 & \cos\chi \end{bmatrix} \tag{18}$$

$$D_\psi = \begin{bmatrix} \cos\psi & \sin\psi & 0 \\ -\sin\psi & \cos\psi & 0 \\ 0 & 0 & 1 \end{bmatrix} \tag{19}$$

$$D_\alpha = \begin{bmatrix} \cos\alpha & 0 & -\sin\alpha \\ 0 & 1 & 0 \\ \sin\alpha & 0 & \cos\alpha \end{bmatrix} \tag{20}$$

$$D_\beta = \begin{bmatrix} 1 & 0 & 0 \\ 0 & \cos\beta & \sin\beta \\ 0 & -\sin\beta & \cos\beta \end{bmatrix} \tag{21}$$

The expression for the angular rates is given by:

$$\boldsymbol{\omega} = \dot{\boldsymbol{\beta}} + \dot{\boldsymbol{\alpha}} + \dot{\boldsymbol{\psi}} + \dot{\boldsymbol{\chi}} \tag{22}$$

$$= \begin{bmatrix} \dot{\beta} \\ 0 \\ 0 \end{bmatrix} + D_\beta \begin{bmatrix} 0 \\ \dot{\alpha} \\ 0 \end{bmatrix} + D_\beta D_\alpha \begin{bmatrix} 0 \\ 0 \\ \dot{\psi} \end{bmatrix} - D_\beta D_\alpha D_\psi \begin{bmatrix} 0 \\ \dot{\chi} \\ 0 \end{bmatrix} \tag{23}$$

$$\begin{bmatrix} \omega_x \\ \omega_y \\ \omega_z \end{bmatrix} = \begin{bmatrix} 1 & 0 & -\mathrm{s}_\alpha \\ 0 & \mathrm{c}_\beta & \mathrm{c}_\alpha \mathrm{s}_\beta \\ 0 & -\mathrm{s}_\beta & \mathrm{c}_\alpha \mathrm{c}_\beta \end{bmatrix} \begin{bmatrix} \dot{\beta} \\ \dot{\alpha} \\ \dot{\psi} \end{bmatrix} - \begin{bmatrix} \mathrm{c}_\alpha \mathrm{s}_\psi \\ \mathrm{s}_\alpha \mathrm{s}_\beta \mathrm{s}_\psi + \mathrm{c}_\beta \mathrm{c}_\psi \\ \mathrm{s}_\alpha \mathrm{c}_\beta \mathrm{s}_\psi - \mathrm{s}_\beta \mathrm{c}_\psi \end{bmatrix} \dot{\chi} \tag{24}$$

This system is then solved for the Euler angular rates to yield:

$$\begin{bmatrix} \dot{\beta} \\ \dot{\alpha} \\ \dot{\psi} \end{bmatrix} = \begin{bmatrix} 1 & \mathrm{s}_\beta \tan\alpha & \mathrm{c}_\beta \tan\alpha \\ 0 & \mathrm{c}_\beta & -\mathrm{s}_\beta \\ 0 & \mathrm{s}_\beta / \mathrm{c}_\alpha & \mathrm{c}_\beta / \mathrm{c}_\alpha \end{bmatrix} \left\{ \begin{bmatrix} \omega_x \\ \omega_y \\ \omega_z \end{bmatrix} + \dot{\chi} \begin{bmatrix} \mathrm{c}_\alpha \mathrm{s}_\psi \\ \mathrm{s}_\alpha \mathrm{s}_\beta \mathrm{s}_\psi + \mathrm{c}_\beta \mathrm{c}_\psi \\ \mathrm{s}_\alpha \mathrm{c}_\beta \mathrm{s}_\psi - \mathrm{s}_\beta \mathrm{c}_\psi \end{bmatrix} \right\} \tag{25}$$

From Vinh,[15] we deduce that

$$\dot{\chi} = \frac{\mu \cos\gamma}{r^2 V} \tag{26}$$

Equations 25 and 26 form the relative attitude equations of motion.

The natural motion of the relative wind angles can be examined by setting $\boldsymbol{\omega}$ to $\mathbf{0}$, and setting the sideslip angle β and roll angle ψ to 0 as well. Equations 25 and 26 collapse to:

$$\begin{bmatrix} \dot{\beta} \\ \dot{\alpha} \\ \dot{\psi} \end{bmatrix} = \begin{bmatrix} 0 \\ \dot{\chi} \\ 0 \end{bmatrix} \tag{27}$$

We note from Eq. 26 that $\dot{\chi} > 0$ during the drag pass. Thus, the angle of attack will naturally tend

to increase as the spacecraft orbits the planet. The exact solution to the attitude EOMs will have an oscillating component, but without any control along the pitch axis, the angle of attack would be biased in the positive direction. From Eq. 14, we conclude that with an uncontrolled attitude, momentum will tend to accumulate along the pitch axis during each drag pass. An attitude control is necessary to prevent the buildup of momentum.

Reaction Wheel Control Laws

The reaction wheel control laws can be divided into two types — exoatmospheric and atmospheric. In exoatmospheric flight, the reaction wheels are commanded to maintain an inertial attitude. For atmospheric flight, we investigate 3 control laws: spin down, affine partial state, and two stage.

Inertial Attitude Hold Controller

In normal spacecraft operation, the spacecraft is held in an inertially fixed attitude to either conduct science experiments or communicate with Earth. In our scheme, the spacecraft prepares for a drag pass by slewing into a new inertially-fixed attitude such that the spacecraft is pointing into the relative wind upon entry. As the spacecraft descends towards periapsis, the angle of attack increases, and the total system angular momentum changes as it is subjected to a growing aerodynamic torque. Since the reaction wheels are commanded to maintain an inertial attitude, the change in momentum is transferred to the reaction wheels. Thus, the spacecraft senses atmospheric entry when the commanded torque magnitude exceeds some threshold. (In our simulations, we use a threshold of 5% maximum torque.) After this threshold is exceeded, the reaction wheel switches to an atmospheric control mode. (Here we note again that the only instrumentation assumed are gyros to measure the angular velocities. It seems clear, however, that an accelerometer would significantly aid in the detection of atmospheric entry.)

Once atmospheric entry is detected, an onboard timer is started. This timer's purpose is to countdown the time until the spacecraft should reach periapsis (which is needed for some control laws) and also to countdown the time until the spacecraft should exit the atmosphere. Upon atmospheric exit, the reaction wheels once again switches modes — this time, back to the inertial attitude hold mode.

These timed events can be predicted by a simple polynomial curve fit, as a function of orbit period. If the atmospheric density is higher or lower than the nominal case, then the sensed entry will be sooner or later than expected, which will slightly alter the timing of events. Timing errors have the largest impact in low-density, high-period orbits since a significant percentage of the flythrough time is used up before atmospheric entry is sensed. A low torque threshold will guard against this kind of timing error (but if the threshold is too small, other perturbations may prematurely activate the atmospheric controller).

Spin-Down Controller

This control law despins the yaw and pitch reaction wheels during the atmospheric flythrough. Upon reaching zero-spin rate, the applied reaction wheel torques are shut off. After exiting the atmosphere, all residual spacecraft momentum is transferred back to the reaction wheels.

This mechanism works because the spacecraft can torque against the atmosphere. The atmosphere tends to keep the spacecraft in place, (the angle of attack and sideslip angles oscillate about zero) while the wheels are desaturated. This control law works best if started near periapsis, where the atmosphere is densest. Before the spacecraft reaches its estimated periapsis, the commanded torque is zero, thus allowing the spacecraft to weathervane (undamped) back and forth into the relative wind. Shortly before periapsis, the pitch and yaw axis reaction wheels are despun at maximum available torque. Afterwards, the commanded torque is again set to zero until exit. To ensure the reaction wheels have enough time to despin, each reaction wheel begins its momentum dump such that the dump will be half completed during the estimated periapsis passage.

Since the roll axis has no opposing external moment to torque against, any change in momentum along that axis will not be altered by the atmosphere. Any momentum storage along the roll axis will either have to be removed propulsively, or by creating an external moment by rotating the solar panels.

This control law has the advantage of being simple to implement, and being independent of spacecraft and planetary parameters. It is also one of the best performing control laws for the six DOF case.

Affine Partial-State Controller

For this approach, we wish to devise a linear state feedback controller to drive the total system momentum to zero. We first need to linearize the attitude EOMs, then pick a feedback gain matrix K to produce a stable closed-loop system, using only the measurable states ($\boldsymbol{\omega}$, $\boldsymbol{\Omega}$) as feedback. The derivation of this controller is as follows:

Linearization of Equations of Motion

The angular momentum from Eq. 6 is a linear combination of the spacecraft and reaction wheel angular rates. The EOMs for the spacecraft angular rates (Eq. 12) is a function of the Euler wind angles. Thus, we need to linearize Eqs. 12, 13, and 25.

The first step in linearization is to choose the desired equilibrium conditions, and to redefine the state variables as appropriate. One such set of equilibrium conditions is:

$$\alpha^e = \beta^e = \psi^e = 0 \tag{28}$$

$$\boldsymbol{\omega}^e = \begin{bmatrix} 0 \\ -\dot{\chi} \\ 0 \end{bmatrix} \tag{29}$$

$$\boldsymbol{\Omega}_{ls}^e = J^{-1}A^T(AA^T)^{-1}I \begin{bmatrix} 0 \\ \dot{\chi} \\ 0 \end{bmatrix} \tag{30}$$

$$\mathbf{u}^e = K_D \boldsymbol{\Omega}^e \tag{31}$$

Let $\mathbf{E}$ be the column vector of Euler angles:

$$\mathbf{E} = \begin{bmatrix} \beta \\ \alpha \\ \psi \end{bmatrix} \tag{32}$$

The state variables are then redefined by subtracting out their equilibrium values. Let $\mathbf{x}$ be the column vector of state variables, and $\delta\mathbf{x} \equiv \mathbf{x} - \mathbf{x}^e$, where $\mathbf{x} \equiv [\mathbf{E}, \boldsymbol{\omega}, \boldsymbol{\Omega}]^T$.

The linearized system of equations can be written as:

$$\delta\dot{\mathbf{x}} = A(\rho)\delta\mathbf{x} + B\delta\mathbf{u} \tag{33}$$

$$\mathbf{H} = C\delta\mathbf{x} \tag{34}$$

Alternatively, we can write the system in affine form using the original state variables as:

$$\dot{\mathbf{x}} = A(\rho)\mathbf{x} + B\mathbf{u} + F \tag{35}$$

$$\mathbf{H} = C\mathbf{x} \tag{36}$$

where

$$A = \begin{bmatrix} -\omega_A^e & 1_{3\times3} & 0_{3\times n} \\ I^{-1}\frac{\partial \mathbf{M}}{\partial \mathbf{E}} & -I^{-1}\omega_A^e I & A_{23} \\ 0_{3\times3} & 0_{3\times3} & -J^{-1}K_D \end{bmatrix} \tag{37}$$

$$A_{23} = I^{-1}(AK_D - \omega_A^e AJ) \tag{38}$$

$$B = \begin{bmatrix} 0_{3\times n} \\ -I^{-1}A \\ J^{-1} \end{bmatrix} \tag{39}$$

$$C = \begin{bmatrix} 0_{3\times3} & I & AJ \end{bmatrix} \tag{40}$$

$$F = \begin{bmatrix} -\boldsymbol{\omega}^e \\ 0_{3\times1} \\ 0_{n\times1} \end{bmatrix} \tag{41}$$

The control law is in the form of $\delta\mathbf{u} = K\delta\mathbf{x}$, or, in terms of original state/control variables:

$$\mathbf{u} = K\mathbf{x} - K\mathbf{x}^e + \mathbf{u}^e \tag{42}$$

K is the feedback control gain of the form

$$K = \begin{bmatrix} K_{\mathbf{E}} & K_{\boldsymbol{\omega}} & K_{\boldsymbol{\Omega}} \end{bmatrix} \tag{43}$$

For a spacecraft with n reaction wheels, we have $6 + n$ states and thus $n^2 + 6n$ feedback gains to choose. Because we cannot measure the Euler angles, we set the $3n$ parameters from $K_{\mathbf{E}}$ to zero. We need a method to pick the remaining $n^2 + 3n$ feedback gains to stabilize the closed-loop system. Since momentum cannot be removed from the roll axis, we set those coefficients to zero. Also, since the pitch and yaw axes are uncoupled in the linearized model, we set the cross terms to zero as well. This leaves us with 4 coefficients to choose (two for the pitch axis, and two for the yaw axis).

Since our A matrix is time-varying, negative instantaneous eigenvalues are insufficient for stability. To achieve stability in the nonlinear time-varying system, we take a minimax approach, where we pick the gain matrix such that the maximum real part of the closed-loop eigenvalues is a minimum. We note that the equilibrium conditions in Eqs. 29 and 30 are functions of $\dot{\chi}$, which is itself a function of the orbit. To avoid having the spacecraft update this parameter after every drag pass, we tune the equilibrium point to the particular orbit corresponding to an eccentricity of 0.4. Alternatively, the equilibrium point could be retuned each orbit, but results indicate that a statically tuned equilibrium point works sufficiently well.

Two-Stage Controller

The affine partial state controller performs nearly all of its work by the time the spacecraft reaches periapsis. In thick atmospheres, the controller quickly drives the system to the equilibrium condition. In thin atmospheres, the affine partial state controller is too sluggish to fully desaturate the reaction wheels. However, the spin-down controller can rapidly despin the wheels. Furthermore, the spin-down controller performs best when activated near periapsis. The advantages of these two controllers inspire us to define a two-stage control law, which is a combination of the two laws. The first stage uses the affine partial state control law, and is activated upon atmospheric entry. The second stage uses the spin-down logic, and is activated at estimated periapsis.

In the cases where the first stage is able to completely remove the system momentum, the spacecraft and reaction wheels have a nonzero equilibrium

Table 2 Reference simulation parameters

Parameter	Reference value
Eccentricity	0.4
Dynamic pressure at periapsis	0.5 N/m^2
Stored momentum[a]	13.5 kg·m^2/s
Entry angle of attack	0 deg
Entry sideslip angle	0 deg

[a] along pitch (+Y) axis

angular rate (Eqs. 29 and 30). We modify the spin-down stage to spin down to the affine partial state equilibrium point. Thus, in the nominal cases, the two-stage controller performs as well as the affine partial state controller.

Results

We judge the effectiveness of a particular control law by the angular momentum reduction achieved during the drag pass. There are several parameters which influence the performance of our control laws. As we consider the variations in the most influential parameters, we find it convenient to establish a set of reference parameters, which are listed in Table 2.

The initial orientation of the stored momentum has a substantial effect. Figure 3 illustrates the fractional momentum remaining after a drag pass (using the two-stage control law) as a function of the direction of the initial stored momentum vector. The color indicates the fractional momentum magnitude remaining, where blue (0%) is the desired result, indicating all stored momentum has been annihilated. The color red (100+%) indicates the spacecraft's momentum magnitude has remained constant or increased as a result of the drag pass. We note that momentum is not removed from the roll (Z) axis, since there are no external moments along that axis. The corresponding plots for the other two control laws (spin-down and affine partial state) yield results very similar to Fig. 3, and are therefore not shown.

The most important parameters that affect our control laws are the atmospheric density and orbit eccentricity. Figures 4, 6 and 8 illustrate the performance of the three control laws. The height of the mesh represents the fractional momentum remaining after a drag pass. The spin-down case (Fig. 4) usually removes about 90% of the stored momentum. It is somewhat less effective in a thin atmosphere. In this case, the spacecraft does not sense atmospheric entry until relatively late in the drag pass. As a result, the periapsis timer is started late, and the spin-down controller barely has enough time to complete

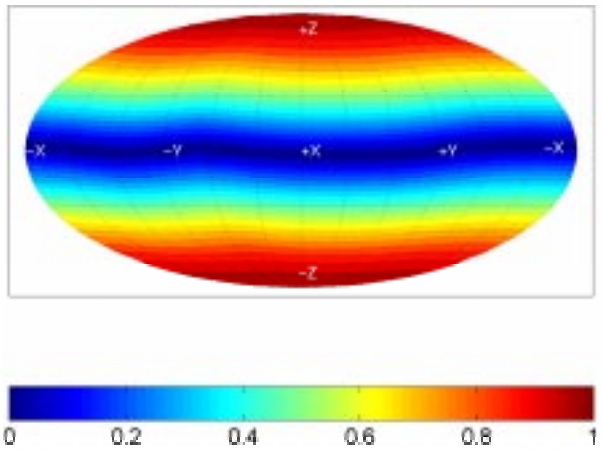

Fig. 3 Fractional momentum remaining after a drag pass as a function of initial momentum orientation, using the two-stage control law.

its momentum dump. However, if the controller is started too early in the nominal or thick atmosphere cases, there will not be enough external torque to oppose the spacecraft's angular momentum. This condition will result in high-amplitude oscillations about the pitch and yaw axes, which will cause the spacecraft to gain momentum instead of to lose it.

The affine partial state control law (Fig. 6) is able to remove nearly 100% of the total momentum in most cases. It has trouble in the low density case, but still works better than the spin down. In the worst case ($\log_{10}\rho/\rho_0 = -1$, $e = 0.9$), spin down removes only 20% of the stored momentum, while the affine partial state removes about 65% of the momentum.

The tuning of the affine partial state about an eccentricity of 0.4 is also evident in Fig. 6 as a slight upward slope in the mesh surface away from the line $e = 0.4$.

Finally, the two-stage control law (Fig. 8) demonstrates the best of both previous controllers. The mesh is flat like the affine partial state, but without the slope. In the worst case, the controller removes over 80% of the stored momentum.

Figures 5, 7, and 9 show another performance characterization. In these plots, the fractional remaining momentum is shown as a function of entry angle of attack (α) and sideslip angle (β). The sideslip angle will typically be known to within a degree, and angle of attack within 15 degrees. All three controllers are able to meet this tolerance in the blue region. In terms of acceptable entry attitudes, the two-stage controller is the most robust, since it performs the best overall, as the entry atti-

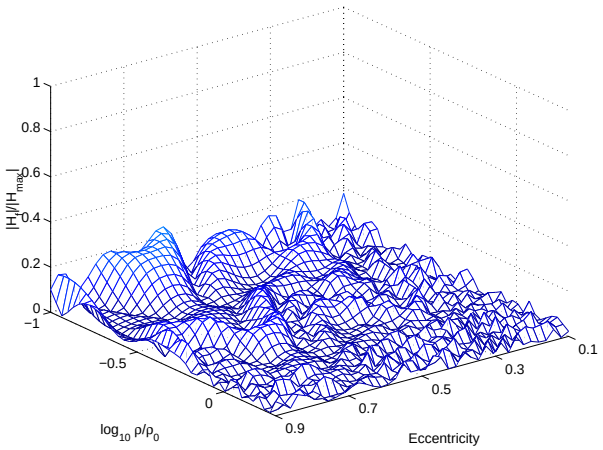

Fig. 4 Fractional momentum remaining after a drag pass for the spin-down controller. Relative density and eccentricity are shown as independent variables. A relative density of 0 is nominal, -1 is 10% nominal, and 0.3 is 200% nominal.

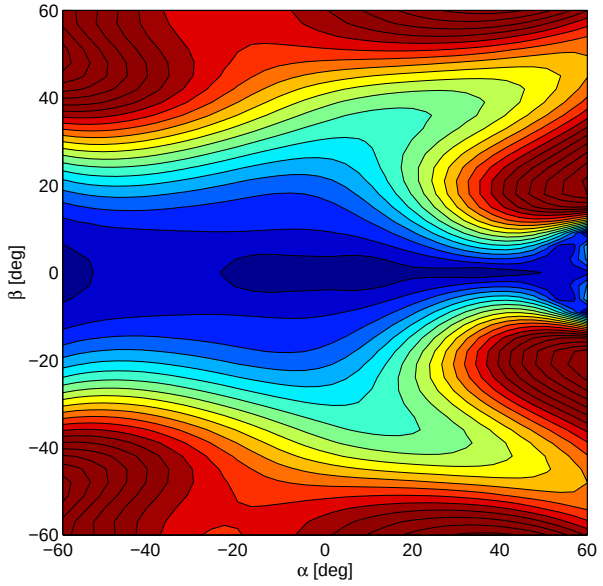

Fig. 5 Fractional momentum remaining after a drag pass for the spin-down controller. Independent variables are angle of attack (α) and sideslip angle (β) at entry.

tude uncertainty increases.

The control laws also perform better with negative entry angles of attack. As the spacecraft orbits the planet, the natural motion (i.e., the tendency for the attitude to remain inertially fixed) causes the angle of attack to increase. Thus, when the spacecraft enters the atmosphere with a high negative α, the atmospheric controller is triggered quickly, and the angle of attack increases naturally. Conversely, with a positive angle of attack at entry, the natural motion is to continue increasing — a behavior which

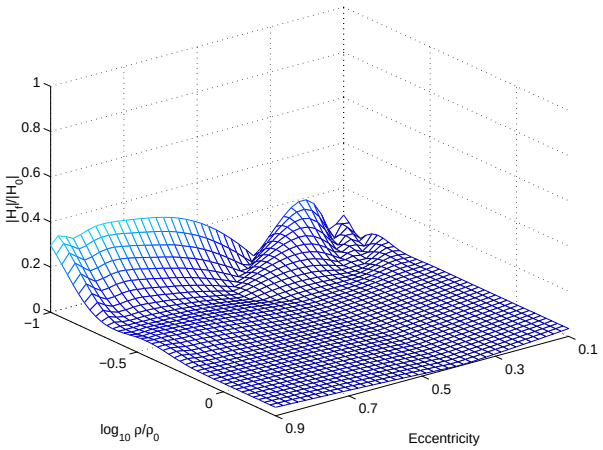

Fig. 6 Fractional momentum remaining using the affine partial state controller.

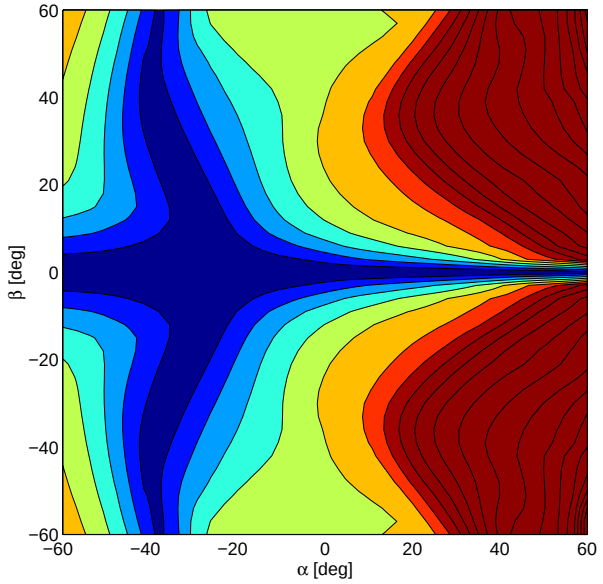

Fig. 7 Fractional momentum remaining using the affine partial state controller.

the spacecraft has difficulty counteracting.

We present an extreme case in Figs. 10-12. These plots show the fractional momentum remaining for the three control laws when the initial momentum wheel (along the pitch axis) is 100% saturated. All three control laws are able to substantially reduce the momentum for every eccentricity and atmospheric density considered.

All three control laws perform well under a variety of conditions. Table 3 summarizes the average and worst-case performance of the three laws. The spin-down and affine partial state controllers have similar performance for low saturations, while the affine partial state is usually better for higher initial saturations. The two-stage controller is uniformly

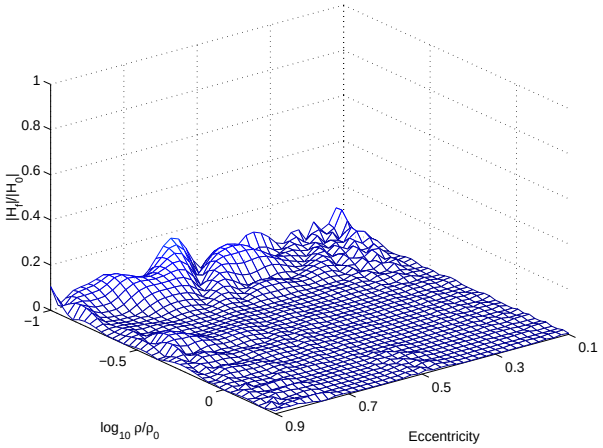

Fig. 8 Fractional momentum remaining using the two-stage controller.

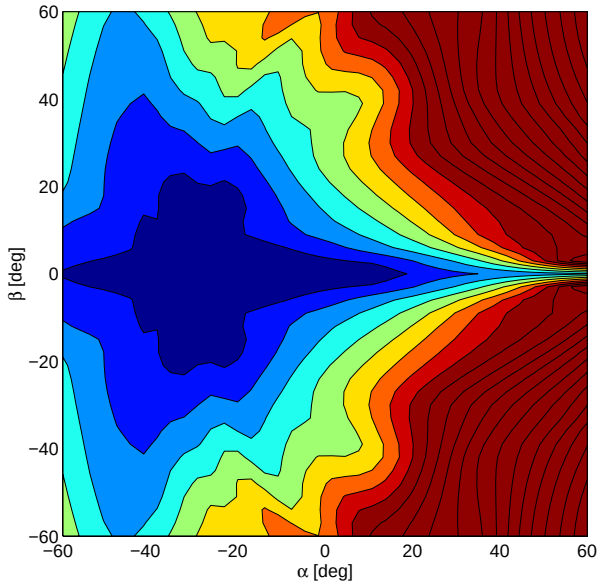

Fig. 9 Fractional momentum remaining using the two-stage controller.

the best control law in almost all test cases.

The Roll Axis

If the solar panels are attached at an angle relative to the $Y - Z$ plane, the relative wind can induce a "propeller torque" on the body +Z axis (the roll axis). Since the torque on the roll axis will always be in same direction, the angular momentum buildup will be secular.

The current practice is to use propellant to manage the spacecraft's momentum. With our two-axis control laws, propellant would only be needed to manage the roll axis momentum. Another scheme to manage the roll axis momentum is to articulate the solar panels to control the rolling moment. This

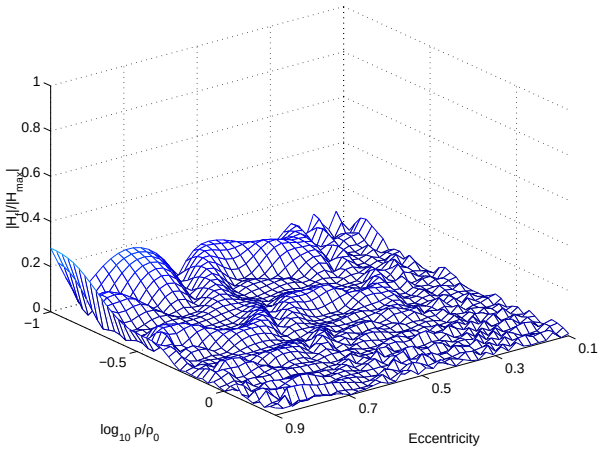

Fig. 10 Fractional momentum remaining using the spin-down controller. Initial stored momentum along the pitch (+Y) axis is 27 kg·m^2/s (100% capacity).

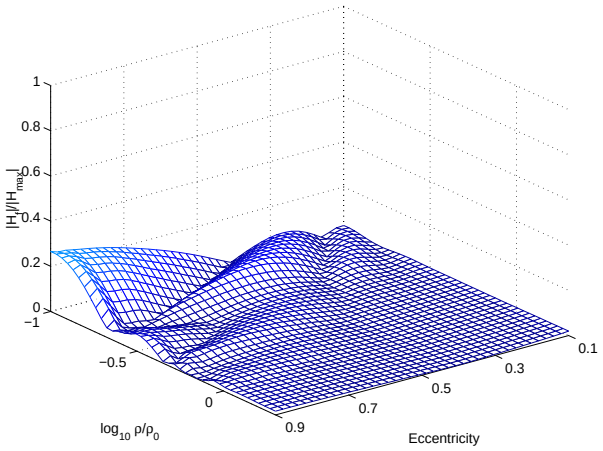

Fig. 11 Fractional momentum remaining using the affine partial state controller.

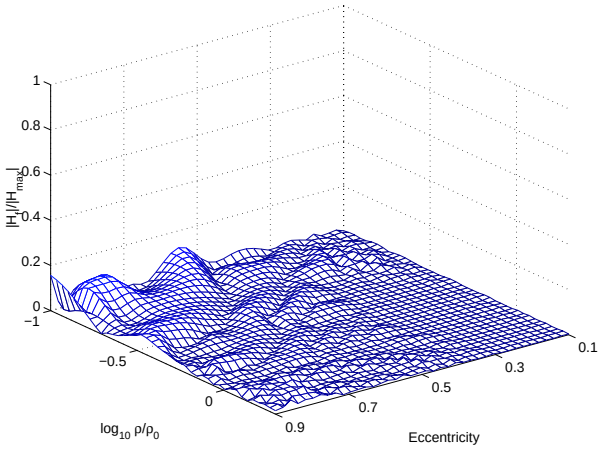

Fig. 12 Fractional momentum remaining using the two-stage controller.

Table 3 Performance summary of control laws

Initial Saturation [%]		Final saturation [%] spin down	affine	two stage
0%	mean	0.9	1.1	0.3
	max	3.1	2.6	1.4
25%	mean	2.9	2.0	1.1
	max	11.1	12.1	6.8
50%	mean	2.5	2.0	0.8
	max	12.2	16.4	8.8
75%	mean	2.6	1.8	1.3
	max	12.6	7.9	9.0
100%	mean	3.6	3.2	2.0
	max	28.2	26.5	15.6

controller would control the pitch angle of the "propellor blades" (solar panels) to first annihilate the roll-axis momentum, and then null out the rolling moment.

Conclusions

All three of the considered control laws are capable of managing the spacecraft angular momentum. The spin-down case is conceptually the simplest of these three control laws, and has the advantage of being independent of spacecraft properties. However, the spin-down controller does require timing information on periapsis, which is particularly critical for high eccentricity orbits and high initial stored momentum.

The affine partial state controller is the easiest to implement, needing only 5 constant parameters to fully describe it. These parameters are functions of spacecraft inertia, aerodynamic moment coefficients, and projected atmospheric density. Since this controller does not require any timing information, it is the least memory-intensive controller of the three.

Finally, the two-stage controller provides performance superior to its two component laws, but at the combined complexity of the two.

Acknowledgments

This work was funded in part by the Purdue Research Foundation and the Jet Propulsion Laboratory, California Institute of Technology, Pasadena, California under JPL Contract No. 1223406 (G. T. Rosalia, Contract Manager and Dennis V. Byrnes, Technical Manager).

Portions of the work described were performed at the Jet Propulsion Laboratory, California Institute of Technology, under contract with NASA.

References

[1]Munk, M. and Powell, R., "Aeroassist Technology Planning for Exploration," *American Astronautical Society*, 2000, AAS 00-169.

[2]Spencer, D. and Braun, R., "Mars Pathfinder Atmospheric Entry: Trajectory Design and Dispersion Analysis," *Journal of Spacecraft and Rockets*, Vol. 33, No. 5, Sept-Oct. 1996, pp. 670–676.

[3]Lyons, D., "Aerobraking at Venus and Mars, a Comparison of the Magellan and Mars Global Surveyor Aerobraking Cases," *AAS/AIAA Astrodynamics Specialist Conference*, Girdwood, AK., August 1999, AAS Paper No 99-358.

[4]Lyons, D., Beerer, J., Esposito, P., Johnston, M., and Willcockson, W., "Mars Global Surveyor: Aerobraking Mission Overview," *Journal of Spacecraft and Rockets*, Vol. 36, No. 3, May-June 1999, pp. 307–313.

[5]Wilmoth, R., Rault, D., Cheatwood, F., and Engelund, W., "Rarefied Predictions for Mars Global Surveyor," *Journal of Spacecraft and Rockets*, Vol. 36, No. 3, May-June 1999.

[6]Lyons, D., "Aerobraking Magellan: Plan Versus Reality," *AAS/AIAA Astrodynamics Specialist Conference*, Feb. 1994, AAS Paper No 94-118.

[7]Tragesser, S. and Longuski, J., "Analysis and Design of Aerocapture Tether with Accounting for Stochastic Errors," *Journal of Spacecraft and Rockets*, Vol. 35, No. 5, Sept.-Oct. 1998, pp. 683–689.

[8]Tragesser, S., *Analysis and Design of Aerobraking Tethers*, Ph.D. thesis, School of Aeronautics and Astronautics, Purdue University, West Lafayette, IN, Dec. 1997.

[9]Lyons, D., "Aerobraking Automation Options," *AAS/AIAA Astrodynamics Specialist Conference*, Aug. 2001, AAS Paper No 01-385.

[10]Johnson, W., Longuski, J., and Lyons, D., "Attitude Control During Autonomous Aerobraking for Near-Term Mars Exploration," *AAS/AIAA Astrodynamics Specialist Conference*, Quebec City, Quebec., Aug. 2001, AAS Paper No 01-388.

[11]Bialke, B., "High Fidelity Mathematical Modeling of Reaction Wheel Performance," *AAS Guidance and Control Conference*, Breckenridge, CO, Feb. 1998, AAS Paper No 98-063.

[12]Justus, C., "Mars Global Reference Atmospheric Model for Mission Planning and Analysis," *Journal of Spacecraft and Rockets*, Vol. 28, No. 2, Mar-Apr 1991, pp. 216–221.

[13]Justus, C. and Johnson, D., "Mars Global Reference Atmospheric Model 2001 Version (Mars-GRAM 2001): Users Guide," Tech. Rep. NASA/TM-2001-210961, 2001.

[14]Davies, M., Abalakin, V., Brahic, A., Bursa, M., Chovitz, B., Lieske, J., Seidelmann, P., Sinclair, A., and Tjuflin, Y., "Report of the IAU/IAG/COSPAR Working Group on Cartographic Coordinates and Rotational Elements of the Planets and Satellites: 1991," *Celestial Mechanics and Dynamical Astronomy*, Vol. 53, 1992, pp. 377–397.

[15]Vinh, N., Busemann, A., and Culp, R., *Hypersonic and Planetary Entry Flight Mechanics*, The University of Michigan Press, Ann Arbor, 1980.